Available online at www.sciencedirect.com
SCIENCE DIRECT®
Sensors and Actuators B xxx (2003) xxx–xxx
SENSORS AND ACTUATORS B CHEMICAL
www.elsevier.com/locate/snb

Synthesis and characterization of sol–gel derived nanocrystalline tin oxide thin film as hydrogen sensor

S. Shukla [a], S. Patil [a], S.C. Kuiry [a], Z. Rahman [a], T. Du [a], L. Ludwig [b], C. Parish [b], S. Seal [a,*]

[a] *Mechanical Materials Aerospace Engineering Department (MMAE), Advanced Materials Processing and Analysis Center (AMPAC), University of Central Florida (UCF), Engineering #381, 4000 Central Florida Blvd., Orlando, FL 32816, USA*
[b] *National Aeronautics and Space Administration (NASA), John F. Kennedy Space Center (KSC), Kennedy Space Center, FL 32899, USA*

Received 4 November 2002; accepted 19 June 2003

Abstract

Tin oxide (SnO_x) semiconductor thin film is coated on Pyrex glass (silica) substrates using the sol–gel dip-coating technique utilizing alkoxide precursor. The thin film is extensively characterized for its surface morphology, chemistry, thickness, and nanocrystallite size using different analytical techniques such as scanning electron microscopy (SEM), X-ray photoelectron spectroscopy (XPS), atomic force microscopy (AFM), and high-resolution transmission electron microscopy (HRTEM). The HRTEM sample preparation is done for the first time using focused ion-beam (FIB) milling technique. Under the given processing conditions, SnO_x semiconductor thin film having thickness 100–150 nm and nanocrystallite size 6–8 nm is obtained. In view of the reported literature and the present experimental data, it is demonstrated that the film is suitable for sensing H_2 gas at room temperature. Sensitivity value as high as 394% is observed at room temperature for 4 vol.% H_2, which is an explosive limit at room temperature for the space-based applications as set by NASA.
© 2003 Elsevier B.V. All rights reserved.

Keywords: Alkoxide; Hydrogen; Nanocrystalline; Sensor; Sol–gel; Tin oxide

1. Introduction

When a polycrystalline Tin oxide (SnO_2) semiconductor thin film is exposed to air, physisorbed oxygen molecules pick up electrons from the conduction band of SnO_2 and change to $O^-_{2(ads)}$ or $O^-_{(ads)}$ species [1]. Consequently, a positive space-charge layer forms just below the surface of SnO_2 particles, which creates a potential barrier between the particles increasing the electrical resistance of the SnO_2 film. However, when a reducing gas comes in contact with the film, it gets oxidized via reaction with the $O^-_{2(ads)}$ or $O^-_{(ads)}$ species and subsequently electrons are reintroduced into the electron depletion layer, leading to decrease in the potential barrier. The sensitivity of the SnO_2 thin film is usually determined by the ratio $(R_a - R_g)/R_g$ (or R_a/R_g), where R_a and R_g are the resistances of the sensor in air and reducing gas, respectively.

SnO_2-based gas sensor has been synthesized in various forms such as thin [2–10] or thick films [11–14] and pellets [15–17]. Thin films are synthesized using sols, which are prepared using either alkoxide [2] or chloride [3] precursors utilizing either dip [2] or spin [3] coating methods. Synthesis of SnO_2 thin films using hydrothermally treated sol [3,4] and other conventional techniques such as ion-assisted deposition [5,6], sputtering [7–10], evaporation [18], chemical vapor deposition [19], spray pyrolysis [20] has been reported. On the other hand, thick films are processed using a paste [11–14] prepared by mixing SnO_2 powder and a binder in a suitable solvent such as water or acetone, which is then applied using screen printing technology [11] on a suitable substrate. Mixing SnO_2 powder with polyvinyl alcohol (PVA) polymer and then pressing the mixed powders into a pellet, which is subsequently sintered at higher temperature, forms pellets [15–17].

However, a lack of consistency in the sensor properties, has been a major problem associated with all these techniques. The processing of SnO_2 semiconductor gas sensor based on pellets or thick film technology are practically excluded from integration in the fabrication of intelligent microsystems, not only due to processing incompatibility but also due to the high power consumption for the gas sensing applications. Thin film technology based on physical methods like vacuum evaporation or sputtering for SnO_2 deposition, combined with ion-implantation for doping the films

* Corresponding author. Tel.: +1-407-823-5277; fax: +1-407-823-0208.
E-mail address: sseal@pegasus.cc.ucf.edu (S. Seal).

0925-4005/$ – see front matter © 2003 Elsevier B.V. All rights reserved.
doi:10.1016/S0925-4005(03)00568-9

with metal ions, are very expensive and may suffer composition inhomogeneity and poor capability to provide good step coverage for topographies with very high aspect ratios. On the other hand, it is well known that the sol–gel technique (used for thin films) has several advantages such as easy control of film thickness, low-cost processing, and ability to produce ultrafine particles, and to coat large complex shapes [21].

The gas sensing properties of SnO_2 semiconductor thin film has been found to depend strongly on the method of processing. Among the structural parameters, the nanocrystallite size [1] and the film thickness [2] have pronounced effect on the gas sensitivity. It is now recognized that SnO_2 semiconductor thin film can have maximum gas sensitivity only if the nanocrystallite size within the film is comparable with its space-charge layer thickness [1]. Hence, the major objectives of the present investigation are set to synthesize SnO_x semiconductor thin film, having nano-scale thickness and nano-sized crystallites (critical parameters for achieving maximum sensitivity) using the sol–gel dip-coating technique utilizing alkoxide precursor. Various analytical techniques such as scanning electron microscopy (SEM), X-ray photoelectron spectroscopy (XPS), atomic force microscopy (AFM), focused ion-beam (FIB), microscopy and high-resolution transmission electron microscopy (HRTEM) are utilized in the present investigation for determining the surface morphology, the chemical composition, the film thickness as well as the nano-crystallite size within the film. The HRTEM analysis of SnO_2 semiconductor thin film using FIB-cut TEM sample is not yet reported in the literature. Besides, the present study also focuses on demonstrating the suitability of such film for sensing H_2 gas at room temperature.

2. Experimental

2.1. Materials

Tin-isopropoxide (10%, w/v) in *iso*-propanol (72 vol.%) and toluene (18 vol.%) was purchased from Aldrich chemicals (USA) and used as-received. Pyrex glass slides, having roughness ±10 nm, were received from Fisher Scientific (USA). Small glass substrates (1 cm × 1 cm), were cut from the glass slides for the dip-coating experiments.

2.2. Sol–gel synthesis of nanocrystalline SnO_x semiconductor thin film

SnO_x (the chemistry is confirmed via XPS, as discussed later) semiconductor thin film coating on the Pyrex glass (silica) slides (substrate) was conducted via sol–gel dip-coating technique. The glass substrates were ultrasonically cleaned, first in acetone and then in *iso*-propanol. The pre-cleaned substrates were dipped in the solution of tin-isopropoxide in *iso*-propanol and toluene, corresponding to the concentration of 0.23 M of tin-isopropoxide, using a dip-coater with a withdrawal speed of 150 cm/min. The gel films were dried at 200 °C for 1 h in air. The substrates were dip-coated again using the same solution under similar conditions and then dried again at 200 °C for 1 h in air. (Note: the dip-coating thickness is estimated to be 50–75 nm after each coating-step.) The dried gel films were fired at 600 °C in air. The samples were heated at a rate of 30 °C/min up to the firing temperature, held at that temperature for 1 h, and then cooled to room temperature inside the furnace. Finally, a thin layer of Pt was sputtered for 5–7 s on some of the semiconductor thin films using a sputter coater (K350, Emitech, Ashford, Kent, England).

2.3. Characterization

All the characterization techniques described below were employed after firing the sol–gel dip-coated SnO_x semiconductor thin films at 600 °C for 1 h.

The surface chemistry of SnO_x thin film dip-coated on the Pyrex glass substrate was studied using XPS technique utilizing PHI ESCA spectrometer (model 5400, Perkin-Elmer, Minnesota), having energy resolution of ±0.1 eV, at a base pressure of 5×10^{-9} Torr using Mg Kα radiation (1253.6 eV). The X-ray power during the analysis was 350 W. Both the survey and the high-resolution narrow-scan spectra were recorded at pass energies of 44.75 and 35.75 eV, respectively, to achieve the maximum spectral resolution. The binding energy (B.E.) of the Au $4f_{7/2}$ at 84.0 ± 0.1 eV was used to calibrate the B.E. scale of the spectrometer. Any charging shifts produced by the samples were carefully removed using a B.E. scale referred to C 1s B.E. of the hydrocarbon part of the adventitious carbon line at 284.6 eV [22]. Non-linear least-squares curve fitting was performed using a Gaussian/Lorentzian peak shape after the background removal [23].

SEM (JSM-6400F, JEOL, Tokyo, Japan) analysis was used to analyze the surface morphology of the dip-coated thin film. To avoid any surface charging during SEM analysis, the SnO_x thin film was coated with approximately 15 nm thick film of Au–Pd using a sputter coater.

The surface morphology of the SnO_x thin film was also studied using AFM (Digital Instrument, USA), utilizing the Si_3N_4 tip of 20 nm radius, in the tapping mode. The average nano-crystallite size within the SnO_x thin film was estimated using AFM.

FIB (FIB 200 TEM, FEI, Hillsboro, OR) milling technique was performed on the SnO_x thin film for TEM sample preparation. The procedure for TEM sample preparation via FIB-milling technique has been described in detail elsewhere [24] and was adopted in the present investigation. It is necessary to mention that the FIB-milling procedure involved first sputtering of 80–100 nm thick Au–Pd layer followed by the deposition of 1 μm thick Pt layer over the SnO_x thin film in order to protect the film from getting destroyed during FIB-milling operation. HRTEM (FEI-Philips Tecnai

F30) was used to study the structure and the nanocrystallite size distribution as well as to observe lattice images showing different orientations of nanocrystals within the SnO_x thin film. Bright field TEM images at 300 kV were taken to observe the lattices. Selected-area electron diffraction (SAED) pattern was collected from the center of the SnO_x thin film to analyze the crystal structure, which also provided the evidence of the presence of nanocrystals having different orientations within the SnO_x thin film.

2.4. Sensor tests

The test set-up (KSC, NASA) used in this investigation was divided into five sections as shown schematically in Fig. 1: (i) electrical contact system for the nanocrystalline SnO_x sensor, which is located inside the chamber and uses edge connectors to make electrical contact with the test-board, (ii) vacuum test chamber, (iii) test gas delivery system for the chamber, which uses control valves and mass flow controllers to deliver a specific quantity of gas into the test-chamber interior, (iv) a residual gas analyzer (RGA) system, which measures the chamber gas composition, and (v) an electrical measurement system, which switches between test specimens and takes the specimens resistance data.

The nano-sensor test system, as schematically shown in Fig. 2(a), is made up of a specimen test-board over which five test samples could be mounted at a time, using a vacuum grade epoxy. A photograph of a test-board is shown in Fig. 2(b). After mounting the sensors (SnO_x and Pt-sputtered SnO_x thin films dip-coated on the glass substrate) on the test-board, conductive Ag-paint was applied for electrical contact purpose. The test-board was installed into the test-chamber and placed in contact with a d.c. voltage heater.

The following procedure was then adopted for the sensor tests. The chamber was first evacuated to 5 Torr pressure and the RGA system was placed into operation to monitor the gas content within the test-chamber. A dry N_2 was purged into the test-chamber allowing the chamber H_2 content to decay. Any residual H_2 from the water vapor was slowly pumped away bringing the H_2 content down to a minimum level. The resistance values were then recorded for each sensor while still maintaining the dry N_2 purge. After stopping the N_2 purge, air at 49.5 standard cubic centimeters per minute (sccm) was introduced into the test-chamber and steady state resistance value was recorded for each sensor. A combination of air and 1 vol.% H_2 was then established and a steady state resistance value was recorded again. This step was repeated for 2, 3, and 4 vol.% H_2 flow rates. The start and stop times of each differing gas flow was recorded so that it could be compared with the RGA output in ppm H_2 with respect to air (or dry N_2). A purge of just breathing air (no H_2) was then performed and the resistance values were

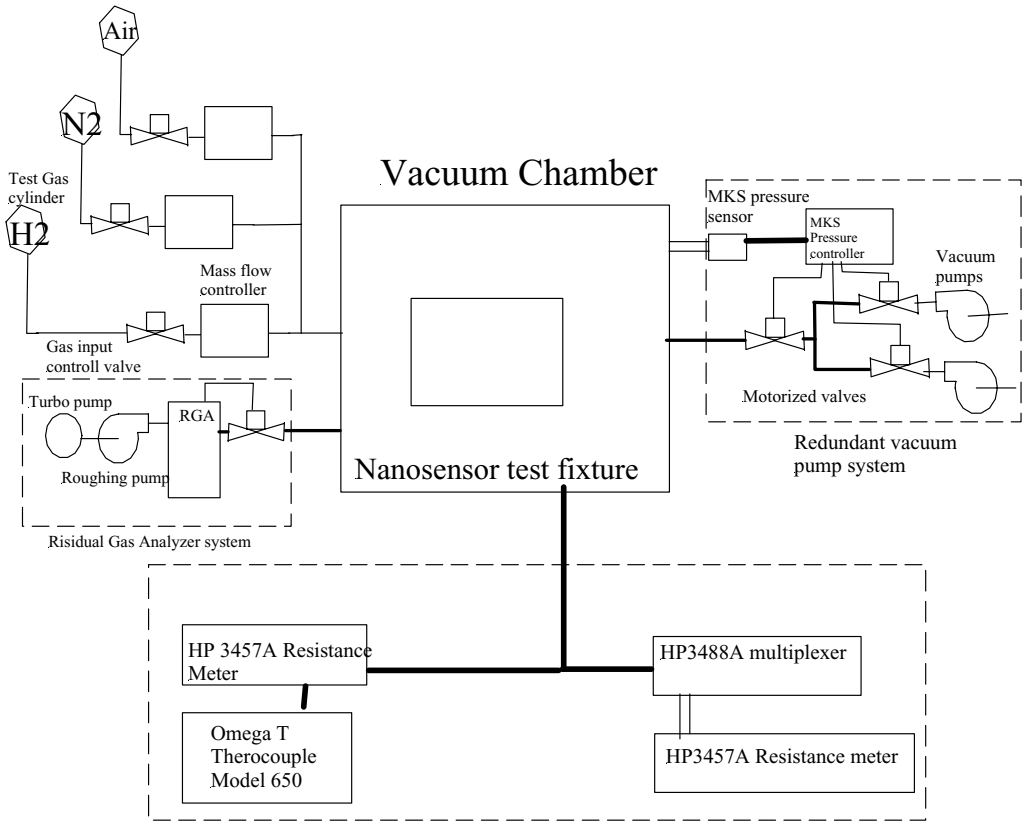

Fig. 1. Schematic diagram describing the set-up used for H_2 sensor test.

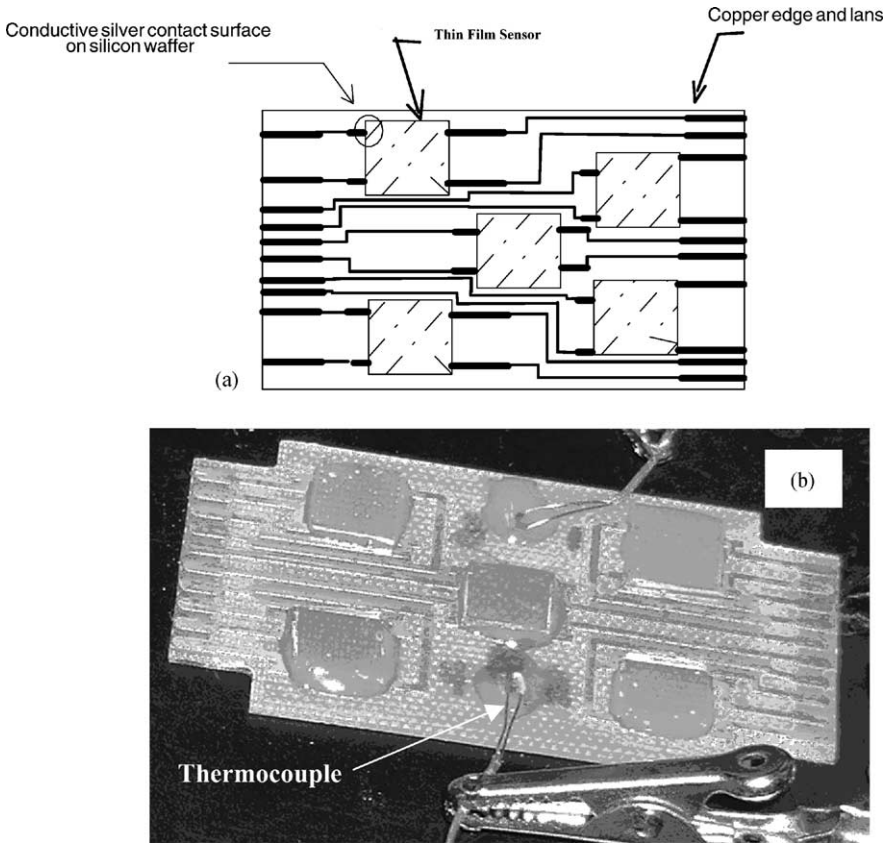

Fig. 2. (a) Schematic diagram describing the design of the test-board and (b) photograph of the test-board with five samples mounted on it.

recorded. This was followed by a purge of N_2 with the final resistance readings were noted. The selection of the range of 1–4 vol.% H_2, in the above test procedure, is based on the NASA's explosive limit of 4 vol.% set for H_2 gas, at room temperature, for the space-based applications.

3. Results

Typical SEM micrographs of Pyrex glass substrate and that of nanocrystalline SnO_x thin film coated on the Pyrex glass substrate are shown in Figs. 3(a) and (b), respectively. The big particle, which is visible in the micrograph, Fig. 3(a), is an artifact and is used for proper focusing of the glass surface. The surface of the glass substrate appears to be very smooth and featureless. Comparison of the glass surface before and after the sol–gel dip-coating process (including the firing treatment), reveals the change in the surface morphology of the glass substrate, which indicates the successful coating of the glass substrate with the semiconductor SnO_x thin film. In Fig. 3(b), the SnO_x thin film appears to be relatively smooth, although at some locations, few cracks are visible on the film surface. Approximately 85–90% of the film surface area was observed to be free of cracks.

Typical broad-scan XPS spectrum, within the B.E. range of 0–1100 eV, obtained for the SnO_x semiconductor thin film dip-coated on the Pyrex glass substrate is shown in Fig. 4(a), which primarily shows the presence of Sn and O on the glass surface after the dip-coating process. Typical narrow-scan analysis of Sn 3d spectra, within the B.E. range of 480–500 eV, is presented in Fig. 4(b). Sn $3d_{5/2}$ B.E. level of 485.8 eV is observed in Fig. 4(b).

Typical AFM image of bare Pyrex glass substrate and those of SnO_x thin film coated on the Pyrex glass substrate, at low and high magnifications, are presented in Figs. 5(a)–(c), respectively. Interestingly, the surface of the glass appears to be smooth even on the nanometer scale level, Fig. 5(a). Comparison of Figs. 5(b) and (c) with (a) shows a change in the surface morphology of the glass substrates after the sol–gel dip-coating process, which is consistent with the SEM observation. From Figs. 5(b) and (c), the SnO_x thin film is observed to be made up of nanoparticles having near-spherical shape and uniform particle size distribution. The average nanoparticle size is estimated to be 15 ± 5 nm, comparable with the resolution limit of AFM, which is determined by the tip radius. Very dense packing of nanoparticles is noted in these micrographs.

Typical TEM images, obtained from the FIB-milled TEM sample of SnO_x thin film dip-coated on the Pyrex glass substrate, are shown in Fig. 6 at different magnifications. The SnO_x thin film thickness measurement is directly possible via these micrographs. Various regions corresponding to Pt,

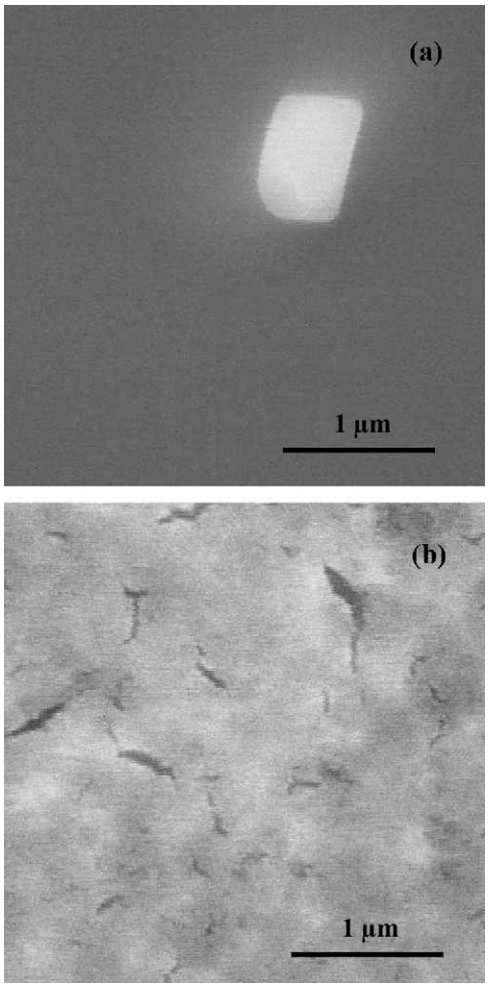

Fig. 3. Typical SEM micrographs showing the surface morphology of Pyrex glass substrate (a) and nanocrystalline SnO_x semiconductor thin film coated on Pyrex glass substrate (b).

Au–Pd (both originating from the FIB-milling procedure), SnO_x (originating from the sol–gel dip-coating process), and the glass substrate are marked appropriately. The SnO_x thin film appears to be smooth and highly continuous. No cracks are visible within the film, although slight variation on the film thickness is noted in these images. The SnO_x thin film thickness is measured to be within the range of ~100–150 nm.

Typical HRTEM images obtained from the different locations of the FIB-milled TEM sample are presented in Figs. 7(a) and (b) at different magnifications. The SAED pattern obtained from the center of the nanocrystalline SnO_x thin film is presented in Fig. 7(c). From these images, it is obvious that the SnO_x thin film is highly dense and nanocrystalline in nature. The SnO_x thin film–glass substrate interface is visible in Fig. 7(a). No porosity or cracks are visible at the interface, which suggests very adherent nature of the sol–gel dip-coated SnO_x thin film. Porosity and cracks are also not observed within the SnO_x thin film even at nano-scale level indicating very dense packing of the nanocrystallites within the thin film, which is in agreement with the AFM analysis. The SnO_x nanocrystallite size of 6–8 nm is observed in the HRTEM image, Fig. 7(b). The nanocrystallite size distribution is thus observed to be very narrow. The SAED pattern, Fig. 7(c), shows continuous and diffused ring pattern, which is an indication of the nanocrystalline nature of the SnO_x thin film.

Typical variation in the H_2 gas sensitivity as a function of the amount of H_2 gas within the range of 1–4 vol.%, observed for the nanocrystalline SnO_x and the Pt-sputtered SnO_x semiconductor thin films, at room temperature and 200 °C, are presented in Figs. 8(a) and (b), respectively. At room temperature, Fig. 8(a), the H_2 gas sensitivity of nanocrystalline SnO_x semiconductor thin film, is observed to increase with increasing amount of H_2 gas. The maximum sensitivity of 394% is observed for 4 vol.% H_2. Nanocrystalline Pt-sputtered SnO_x semiconductor thin film is observed to be insensitive, at room temperature, to any amount of H_2 gas within the investigated range. However, at higher temperature (200 °C), Fig. 8(b), the Pt-sputtered SnO_x thin film becomes sensitive to H_2 gas; the sensitivity is observed to increase with increasing the amount of H_2. The maximum sensitivity of 126% is observed for 4 vol.% H_2. At 200 °C, the nanocrystalline SnO_x semiconductor thin film, exhibits increased sensitivity to lower amount of H_2 (1–2 vol.%). Maximum H_2 gas sensitivity of 94% is observed for 1 vol.% H_2. The sensitivity is, however, observed to reduce for higher amount of H_2 (3–4 vol.%).

4. Discussion

4.1. Synthesis of nanocrystalline SnO_x semiconductor thin film

Nanocrystalline semiconductor SnO_x thin film having the thickness and the nanocrystallite size within the range of 100–150 nm and 6–8 nm, respectively, has been successfully synthesized in this investigation using the sol–gel dip-coating process utilizing the solution of tin isopropoxide in propanol and toluene. In this method, the formation of SnO_x thin film involves hydrolysis of tin-isopropoxide via reaction with the atmospheric moisture on the Pyrex glass substrate, which results in the formation of $Sn(OH)_4$ gel. This gel undergoes condensation reaction upon drying at 200 °C to form a film of amorphous SnO_x particles. The amorphous SnO_x thin film crystallizes upon firing at 600 °C. The sequence of chemical reactions during gelling, drying, and crystallization, for the film having stoichiometric composition, can be summarized as

$$Sn(OC_3H_7)_4 + 4H_2O \rightarrow Sn(OH)_4 + 4C_3H_7OH \quad (\text{at } 25\,^\circ\text{C}) \tag{1}$$

$$Sn(OH)_4 \rightarrow SnO_{2(\text{amorphous})} + 2H_2O \quad (\text{at } 200\,^\circ\text{C}) \tag{2}$$

$$SnO_{2(\text{amorphous})} \rightarrow SnO_{2(\text{crystalline})} \quad (\text{at } 600\,^\circ\text{C}) \tag{3}$$

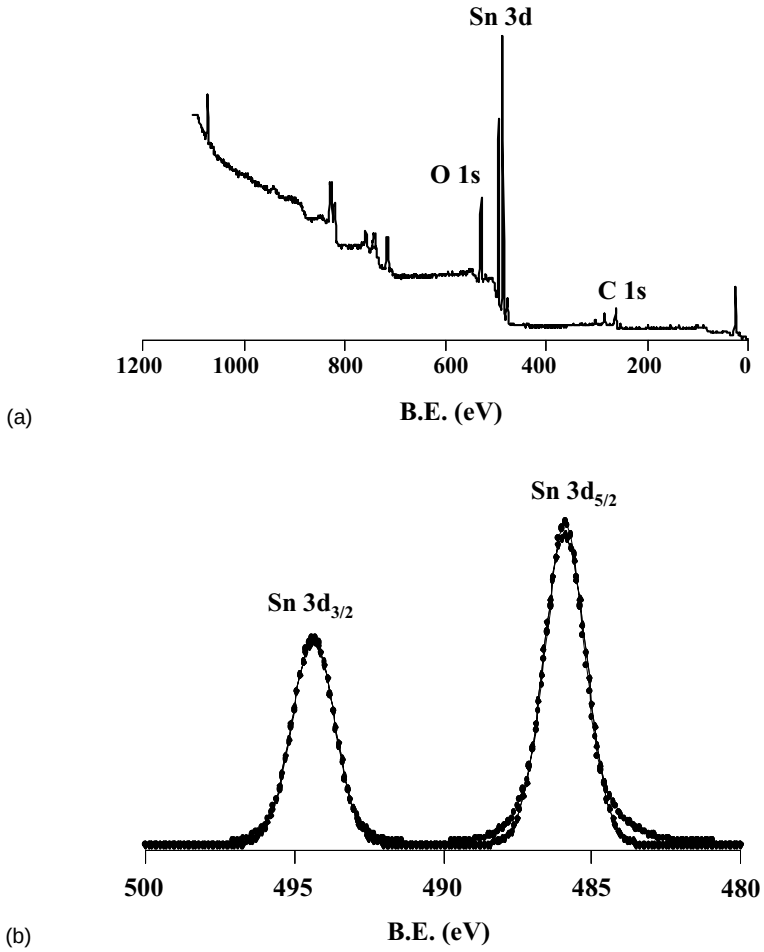

Fig. 4. (a) Broad-scan XPS analysis of nanocrystalline SnO_x semiconductor thin film coated on Pyrex glass substrate. (b) Narrow-scan XPS analysis of Sn 3d within the B.E. range of 480–500 eV.

The SnO_x thin film obtained after firing at 600 °C is a conducting film as well as it is nanocrystalline in nature. The nanocrystalline nature of the film is the most important aspect of the present synthesis method in order to utilize this film for H_2 gas sensing.

In the present investigation, Sn $3d_{5/2}$ B.E. value of 485.8 eV is observed, which is in between the Sn $3d_{5/2}$ B.E. values of 484.9 and 486.7 eV reported for pure-Sn and SnO_2 [25]. Hence, the observed Sn $3d_{5/2}$ B.E. value of 485.8 eV is attributed to the presence of Sn-oxidation state less than +4. The O:Sn relative atomic concentration ratio of ∼1.6 is calculated from the survey spectrum and is in agreement with Sn $3d_{5/2}$ B.E. value. The non-stoichiometric O:Sn ratio suggests the presence of oxygen vacancies [26], which is responsible for the n-type semiconductor property of the film.

4.2. Gas sensitivity and nanocrystallinity

The present nanocrystalline SnO_x semiconductor thin film coated on the Pyrex glass substrate is synthesized to detect H_2 at room temperature. The feasibility of utilizing this nanocrystalline SnO_x semiconductor thin film having thickness 100–150 nm and nanocrystallite size 6–8 nm for H_2 gas sensing is determined here. The usefulness of nanocrystalline SnO_2 semiconductor in various forms for H_2 gas sensing has been demonstrated earlier by many investigators [2–8,10–17,27–30]. In Fig. 9(a), we plot the sensitivity (R_a/R_g) of SnO_2 semiconductor thin film as a function of film thickness [3,4,7,10,28], independent of the values of other variables. The graph shows that the sensitivity of SnO_2 semiconductor thin film increases gradually as the film thickness decreases within the range of 80–400 nm. The upper and lower limits of the gas sensitivity values are observed for the thickness range of 80–200 nm and are attributed to the different processing and test conditions used for obtaining these data points. Moreover, the maximum sensitivity is observed at 80 nm thickness, below which the H_2 gas sensitivity decreases. Such a variation in the gas sensitivity as a function of film thickness has been reported earlier for sensing H_2S gas by Park and Mackenzie [2] and was explained on the basis of single crystal thin film model. The drop in the sensitivity below 80 nm film thickness was attributed to the reduction in the amount of porosity of the

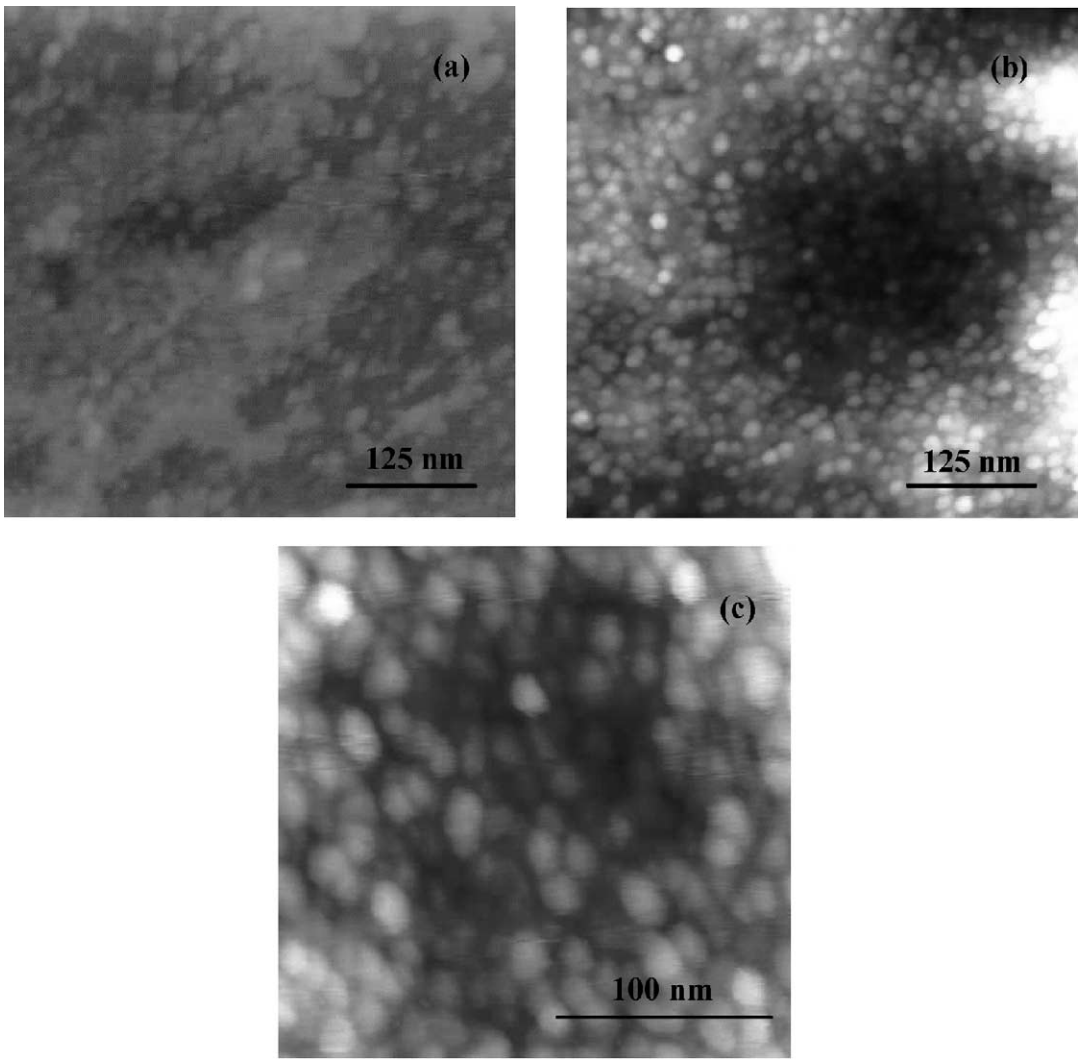

Fig. 5. Typical AFM micrographs showing the surface morphology of Pyrex glass substrate (a) and nanocrystalline SnO_x semiconductor thin film coated on Pyrex glass substrate at low (b) and high (c) magnifications.

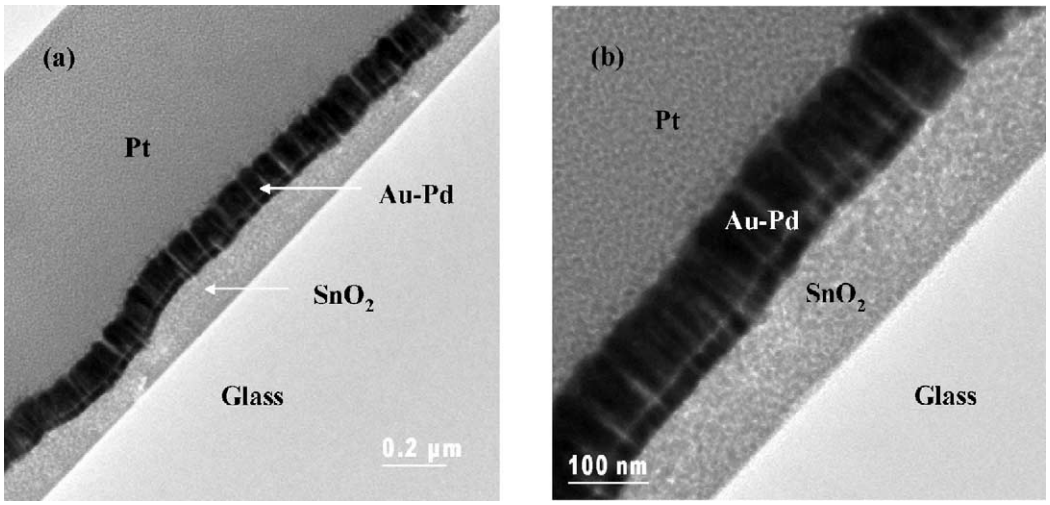

Fig. 6. Typical TEM images of FIB-milled TEM sample, obtained from nanocrystalline SnO_x semiconductor thin film coated on Pyrex glass substrate, at different magnifications.

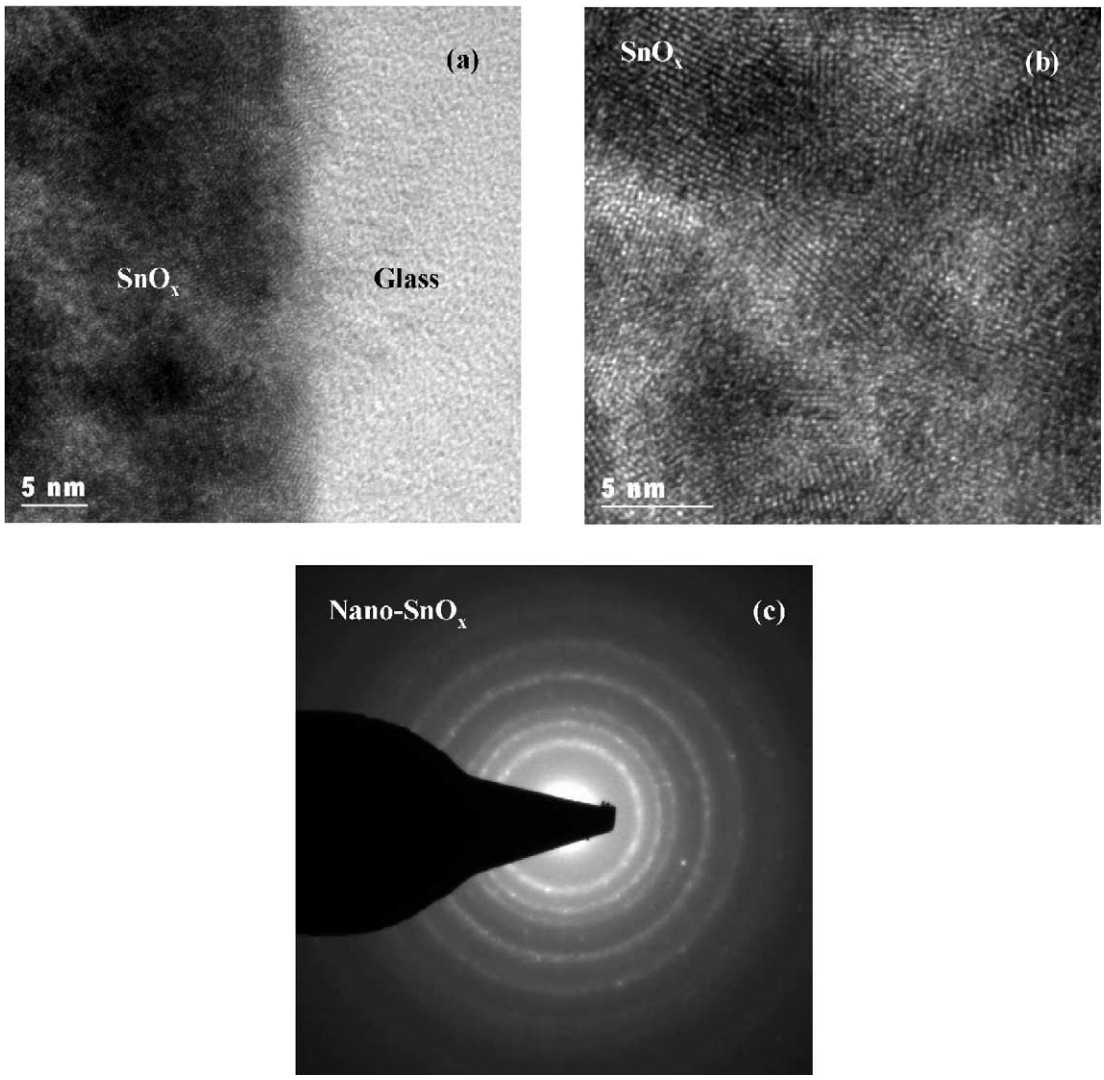

Fig. 7. (a) and (b) Typical HRTEM images of nanocrystalline SnO_x semiconductor thin film coated on Pyrex glass substrate at different locations and magnifications. (c) SAED pattern obtained from the center of the SnO_x thin film coated on Pyrex glass substrate.

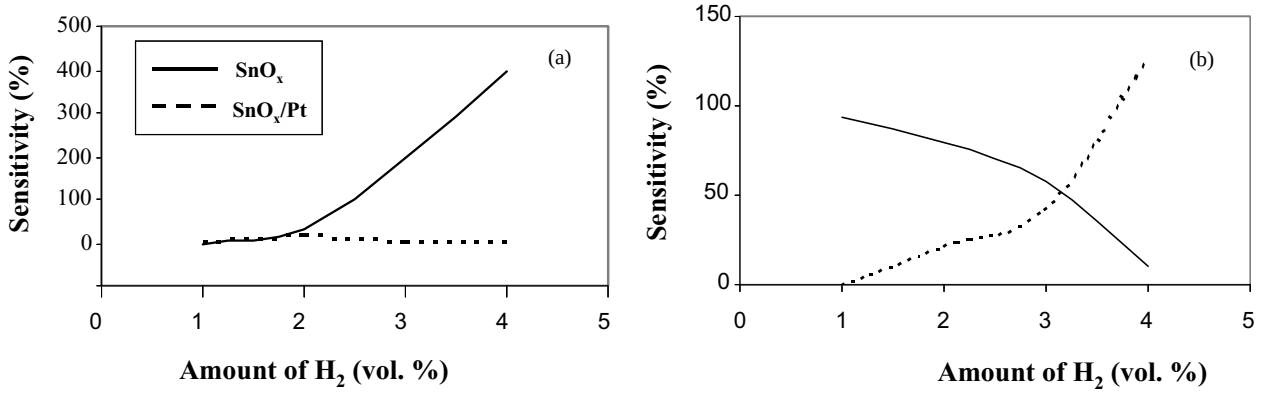

Fig. 8. Variation in the H_2 gas sensitivity $((R_a - R_g)/R_g \times 100)$ as a function of amount of H_2 gas observed at: (a) room temperature and (b) 200 °C.

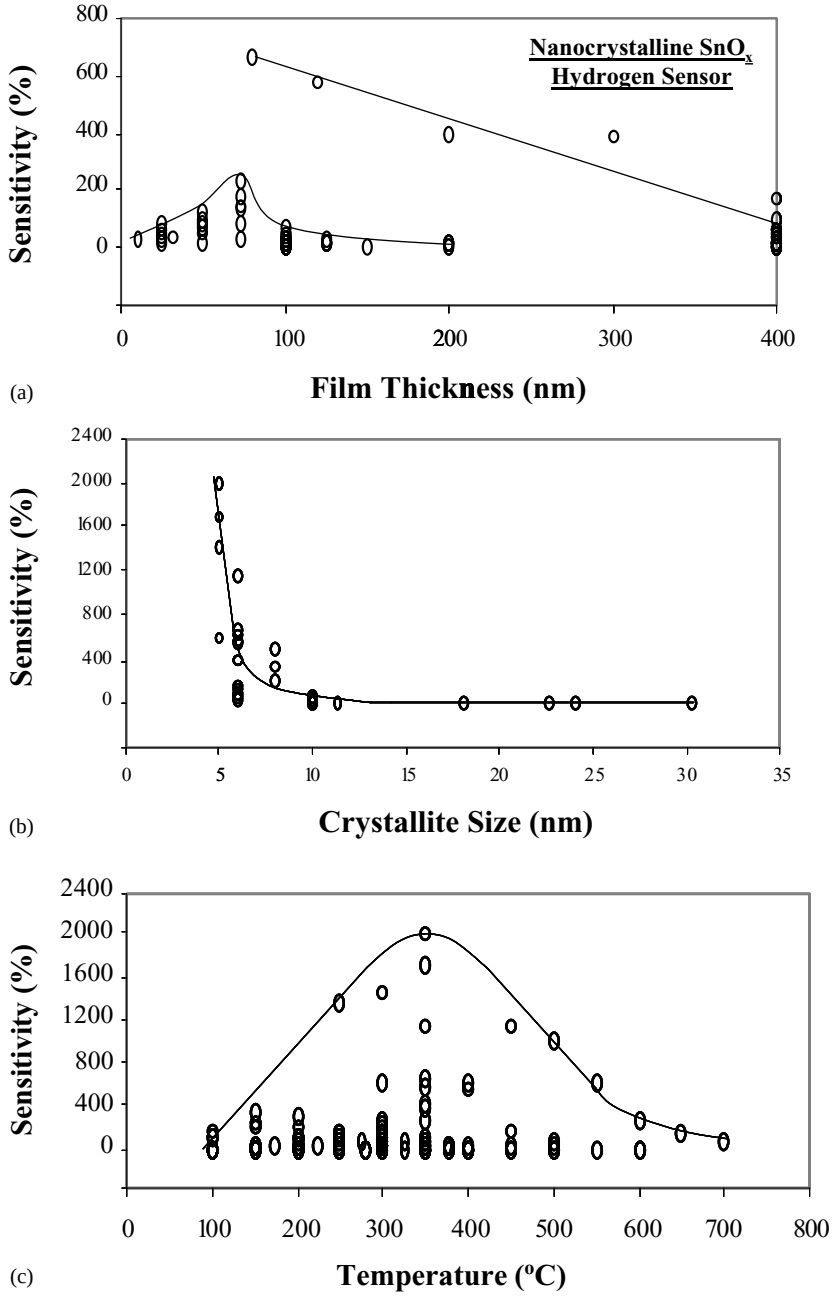

Fig. 9. Graphs of H_2 gas sensitivity as a function of (a) nanocrystalline SnO_2 semiconductor thin film thickness [3,4,7,10,28], (b) SnO_2 nanocrystallite size [4,7,12,29] and (c) operating temperature [7,8,10,13,29,30].

SnO_2 semiconductor thin film [2]. In the present investigation, the obtained film thickness of 100–150 nm is very close to the range where maximum H_2 gas sensitivity is observed, Fig. 9(a).

In Fig. 9(b), we plot the H_2 gas sensitivity of nanocrystalline SnO_2 as a function of crystallite size [4,7,12,29], independent of the values of other variables. The graph shows that above nanocrystallite size of 10 nm, the H_2 gas sensitivity of nanocrystalline SnO_2 semiconductor thin film is low and almost independent of average nanocrystallite size. However, the sensitivity increases gradually first as the nanocrystallite size decreases below 10 nm and then sharply below 6 nm. Very high surface area and the operation of 'grain-size-control' mechanism [1], which primarily determines the electrical resistance of the film, are responsible for very high H_2 gas sensitivity values below 6 nm crystallite size. In the present investigation, the nanocrystallite size range of 6–8 nm is observed, which is also close to the nanocrystallite size range where very large H_2 gas sensitivity is observed. It appears that, both the film thickness and the nanocrystallite size of the sol–gel dip-coated nanocrystalline SnO_x thin film, synthesized in the present investigation, are

close to the optimum values to achieve maximum H_2 gas sensitivity.

The variation in H_2 gas sensitivity of nanocrystalline SnO_2 film as a function of operating temperature is plotted in Fig. 9(c) [7,8,10,13,29,30], independent of the values of other variables. The graph shows that, within the temperature range of 100–700 °C, the H_2 gas sensitivity increases initially with increasing operating temperature. The maximum sensitivity is observed at 350 °C. The sensitivity, however, decreases with further increase in the operating temperature above 350 °C. The graph indicates that the room temperature H_2 gas sensitivity of nanocrystalline SnO_2 semiconductor thin film is extremely low, which is primarily due to extremely low reaction kinetics between the H_2 gas and the oxygen adsorbates. The reaction kinetics improves with increasing operating temperature, thus increasing the sensitivity. At higher operating temperature, instability in the microstructure (grain size) results in the loss of H_2 gas sensitivity.

4.3. Sensing H_2 gas at room temperature

H_2 gas, when comes in contact with the nanocrystalline SnO_x semiconductor thin film, gets dissociated (which generally requires higher temperature or a catalyst for activation) into hydrogen atoms, which get adsorbed on the film surface. They diffuse towards O^- adsorbates, releasing water and an electron after the reaction, which increases the conductivity of the film. The reactions can be summarized as

$$H_{2(g)} \rightarrow H_{(ads)} + H_{(ads)} \quad (4)$$

$$H_{(ads)} + H_{(ads)} + O^-_{(ads)} \rightarrow H_2O + e^- \quad (5)$$

Due to very low decomposition rate of H_2 gas, very low sensitivity values are reported in the literature, Fig. 9(c), for sensing H_2 gas at ppm level at room temperature. In this investigation, the sensitivity tests were conducted for relatively large amount of H_2 gas within the range of 1–4 vol.%. We observe that, in this range, the nanocrystalline SnO_x semiconductor thin film is sensitive to H_2 at room temperature. However, nanocrystalline SnO_x semiconductor thin film sputtered with a thin layer of Pt is observed to be insensitive to H_2 at room temperature. It is known that the presence of a catalyst (Au, Pd, or Pt) aid in the catalytic decomposition of H_2, thus increasing the sensitivity of SnO_2 semiconductor thin film [31]. It is to be noted that, in the present investigation, the Pt is sputtered after calcining the dip-coated SnO_x thin film at higher temperature. As a result, sputtered-Pt possibly remained as a thin amorphous layer on the SnO_x thin film during testing at room temperature. Sputtered-Pt in a form of crystalline particles having extremely small size, rather than a continuous amorphous layer, is expected to be more effective for catalytic applications [32]. The continuous amorphous Pt layer is not only ineffective from the point of view of H_2 decomposition but also acting as a barrier for direct contact between the H_2 gas and the nanocrystalline SnO_x semiconductor thin film. This has resulted in the loss of sensitivity for the Pt-sputtered nanocrystalline SnO_x semiconductor thin film at room temperature. The enhanced sensitivity for the same Pt-sputtered nanocrystalline SnO_x semiconductor thin film at 200 °C is possibly due to the transformation of continuous amorphous layer of Pt layer into agglomerated Pt nanoparticles [32], which may allow the direct interaction between the H_2 gas and the sensor surface. The decrease in the sensitivity observed for the nanocrystalline SnO_x semiconductor thin film at 200 °C is, however, abnormal, which is attributed to the instability in the microstructure (grain size) of nanocrystalline SnO_x semiconductor thin film due to continuous exposure to high temperature during testing.

It is thus shown that the nanocrystalline (6–8 nm) SnO_x semiconductor thin film (100–150 nm) can sense H_2 gas (1–4 vol.%) at room temperature. It is noted that there are several other issues, such as selectivity, minimum response and recovery time, reproducibility, stability, and room temperature sensing at ppm level, associated with the H_2 gas sensing using SnO_x semiconductor thin film sensor. Some of these aspects of H_2 gas sensing will be reported in the next communication. The present investigation, however, clearly shows the significance of the sol–gel dip-coating technique in producing the nanocrystalline SnO_x semiconductor thin film having optimum thickness and nanocrystallite size required for sensing H_2 gas at room temperature.

5. Conclusions

(1) SnO_x (where x is observed to be 1.6 by XPS) semiconductor thin film having thickness 100–150 nm and average nanocrystallite size 6–8 nm have been successfully synthesized using sol–gel dip-coating technique utilizing alkoxide precursor and characterized completely using SEM, AFM, XPS, FIB, and HRTEM.

(2) It is demonstrated in view of the available literature and the present experimental data that this nanocrystalline SnO_x semiconductor thin film is suitable for H_2 (1–4 vol.%) gas sensing at room temperature useful for space-based applications.

Acknowledgements

The authors thank UCF, Florida Space Grant Consortium, FSEC (NASA Glenn), NASA, National Science Foundation (NSF EEC 0136710) for funding the sensor and nano-technology research.

References

[1] S. Seal, S. Shukla, Nanocrystalline SnO gas sensors in view of surface reactions and modifications, JOM 54 (9) (2002) 35–38, 60.

ARTICLE IN PRESS

[2] S.-S. Park, J.D. Mackenzie, Thickness and microstructure effects on alcohol sensing of tin oxide thin films, Thin Solid Films 274 (1996) 154–159.
[3] G. Sakai, N.S. Baik, N. Miura, N. Yamazoe, Gas sensing properties of tin oxide thin films fabricated from hydrothermally treated nanoparticles, Sens. Actuators B 77 (2001) 116–121.
[4] N.S. Baik, G. Sakai, N. Miura, N. Yamazoe, Hydrothermally treated sol solution of tin oxide for thin film gas sensor, Sens. Actuators B 63 (2000) 74–79.
[5] W.K. Choi, S.K. Song, J.S. Cho, Y.S. Yoon, D. Choi, H.-J. Jung, S.K. Koh, H_2 gas-sensing characteristics of SnO_x sensors fabricated by a reactive ion-assisted deposition with/without an activation layer, Sens. Actuators B 40 (1997) 21–27.
[6] S.-K. Song, J.-S. Cho, W.-K. Choi, H.-J. Jung, D. Choi, J.-Y. Lee, H.-K. Baik, S.-K. Koh, Structure and gas-sensing characteristics of undoped tin oxide thin films by ion-assisted deposition, Sens. Actuators B 46 (1998) 42–49.
[7] K.H. Cha, H.C. Park, K.H. Kim, Effect of palladium doping and film thickness on the H_2-gas sensing characteristics of SnO_2, Sens. Actuators B 21 (1994) 91–96.
[8] G. Sberveglieri, G. Faglia, S. Groppelli, P. Nelli, Methods for the preparation of NO, NO_2 and H_2 sensors based on tin oxide thin films, grown by means of the r.f. magnetron sputtering technique, Sens. Actuators B 8 (1992) 79–88.
[9] H.-J. Michel, H. Leiste, K.D. Schierbaum, J. Halbritter, Adsorbates and their effects on gas sensing properties of sputtered SnO_2 films, Appl. Surf. Sci. 126 (1998) 57–64.
[10] V.V. Malyshev, A.A. Vasiliev, A.V. Eryshkin, E.A. Koltypin, Y.I. Shubin, A.I. Buturlin, V.A. Zaikin, G.B. Chakhunashvili, Gas sensitivity of SnO_2 and ZnO thin-film resistive sensors to hydrocarbons, carbon monoxide and hydrogen, Sens. Actuators B 10 (1992) 11–14.
[11] V.N. Mishra, R.P. Agarwal, Thick-film hydrogen sensor, Sens. Actuators B 21 (1994) 209–212.
[12] G.S. Devi, S.K. Masthan, M. Shakuntalav, J. Rao, Correlation between structural properties and gas sensing characteristics of SnO_2 based gas sensors, J. Mater. Sci.: Mater. Electron. 10 (1999) 545–549.
[13] Y. Shimizu, Y. Nakamura, M. Egashira, Effects of diffusivity of hydrogen and oxygen through pores of thick film SnO_2 based on their sensors properties, Sens. Actuators B 13–14 (1993) 128–131.
[14] A. Katsuki, K. Fukui, H_2 selective gas sensor based on SnO_2, Sens. Actuators B 52 (1998) 30–37.
[15] V. Jayaraman, K.I. Gnanasekar, E. Prabhu, T. Gnanasekaran, G. Periaswami, Sens. Actuators B 55 (1999) 147–153.
[16] V.A. Chaudhary, I.S. Mulla, K. Vijayamohanan, Selective hydrogen sensing properties of surface functionalized tin oxide, Sens. Actuators B 55 (1999) 154–160.
[17] V.A. Chaudhary, I.S. Mulla, K. Vijayamohanan, Comparative studies of doped and surface modified tin oxide towards hydrogen sensing: synergistic effects of Pd and Ru, Sens. Actuators B 50 (1998) 45–51.
[18] G.F. Carbajal, A.S. Tiburcio, J.M. Sanchez, Thin film tin oxide-based propane gas sensors, Thin Solid Films 373 (1–2) (2000) 141–144.
[19] J.R. Brown, P.W. Haycock, L.M. Smith, A.C. Jones, E.W. Williams, Response behavior of tin oxide thin film gas sensors grown by MOCVD, Sens. Actuators B 63 (1) (2000) 109–114.
[20] R.S. Niranjan, S.R. Sainkar, K. Vijayamohanan, I.S. Mulla, Ruthenium:tin oxide thin film as a highly selective hydrocarbon sensor, Sens. Actuators B 82 (1) (2002) 82–88.
[21] L. Klein, Sol–gel technology for thin films, fibers, preforms, electronics, and specialty shapes, Part II, Park Ridges, NJ, 1988.
[22] T.L. Barr, S. Seal, Nature of the use of adventitious carbon as a binding energy standard, J. Vac. Sci. Technol. A 13 (3) (1995) 1239–1246.
[23] P.M.A. Sherwood, in: D. Briggs, M.P. Seah (Eds.), Practical Surface Analysis: Auger and Photoelectron Spectroscopy, vol. 1, 2nd ed., Wiley, New York, 1996, p. 555 (Appendix 3).
[24] B.I. Prenitzer, L.A. Giannuzzi, K. Newman, S.R. Brown, R.B. Irwin, T.L. Shoftner, F.A. Stevie, Transmission electron microscope specimen preparation of Zn powders using focused ion beam lift-out technique, Metall. Mater. Trans. A 29 (9) (1998) 2399–2406.
[25] J.F. Moulder, W.F. Stickle, P.E. Sobol, K.D. Bomben, in: J. Chastain (Ed.), Handbook of X-ray Photoelectron Spectroscopy: A Reference Book of Standard Spectra for Identification and Interpretation of XPS Data, Perkin-Elmer Corporation, Physical Electronics Division, Minnesota.
[26] S.P. Lee, Analysis of SnO_{2-x}/Pt thin film for gas sensors, Sens. Actuators B 15–16 (1993) 379–383.
[27] Y.-D. Wang, C.-L. Ma, X.-H. Wu, X.-D. Sun, H.-D. Li, Electrical and gas sensing properties of mesostructured tin oxide-based H_2 sensor, Sens. Actuators B 85 (2002) 270–276.
[28] J. Zhang, K. Colbow, Surface silver clusters as oxidation catalysts on semiconductor gas sensor, Sens. Actuators B 40 (1997) 47–52.
[29] N.S. Baik, G. Sakai, K. Shimanoe, N. Miura, N. Yamazoe, Hydrothermal treatment of tin oxide sol solution for preparation of thin-film sensor with enhanced thermal stability and gas sensitivity, Sens. Actuators B 65 (2000) 97–100.
[30] S. Matsushima, T. Maekawa, J. Tamaki, N. Miura, N. Yamazoe, New methods for supporting palladium on a tin oxide gas sensor, Sens. Actuators B 9 (1992) 71–78.
[31] A. Cabot, A. Dieguez, A.R. Rodriguez, J.R. Morante, N. Barsan, Influence of the catalytic introduction procedure on the nano-SnO_2 gas sensor performances where and how stay the catalytic atoms? Sens. Actuators B 79 (2001) 98–106.
[32] J. Mizsei, L. Pirttiaho, M. Karppinen, V. Lantto, Nanocatalyst sensitizers by agglomeration of nanofilms, Sens. Actuators B 65 (2000) 195–198.